Biophysical Principles of Avian High-Speed Wing Architecture: Implications on Aerodynamic and Aeroelastic Improvements for Small Unmanned Aerial Vehicles

Hanyue Shen[1]

[1]Shanghai Pinghe School, Shanghai, People's Republic of China
shenhanyue@shphschool.com

Abstract – This research discusses and analyzes the aerodynamic and aeroelastic properties of a biomimetic parametrized optimization design based on the high-speed wings of peregrine falcons. The design process uses the VLM method and PSO algorithms to obtain rapid optimizations, then engages fluid and structural finite element analysis to predict more complicated elastic properties and validates the results with two separate wind tunnel experiments in CWT and micro desktop wind tunnel. Under simulation conditions, the optimized design shows an over 5% decrease in displacement, an over 8.8% decrease in total strain, and a 20.10% decrease in high aerodynamic loading area compared to the straight delta wing with equivalent conditions. These conclusions are supported by experimental results, demonstrating the potential of utilizing this configuration on small drones to achieve high maneuverability with lighter structures while ensuring cruise efficiency. It is valuable to small drones as it will allow them to carry out more complicated and demanding missions without increasing their cost and size.

Keywords: Biomimetic Design, Aerodynamics, Aeroelasticity, Finite Element Analysis

Abbreviations and Conventions		
Full Name	***Abbrev.***	***Standard Unit***
Aspect Ratio	AR	/
Attack Angle	α/a.o.a.	**deg**
Bending Moment	BM	**N/m**
Coefficient of Lift	CL	/
Coefficient of Drag	CD	/
Coefficient of Moment	Cm	/
Lift-Drag Ratio	L/D	/
Maximum Takeoff Weight	MTOW	**g**
Sideslip Angle	β	**deg**
Sheer Stress	τ	**Pa**
Static Displacement	URES	**mm**
Velocity (Stall)	VS	**m/s**
Velocity (Cruise)	VC	**m/s**
Velocity (Never Exceeding)	VNE	**m/s**
Vortex-Lattice Method	VLM	/
Von Mises Stress	vM	**Pa**

1. Introduction

Since the beginning of human flight, there has been a continuous yearning for better flight performance. In many cases, inspiration for these improvements comes from the natural residents of the sky.

Studies on designs have concluded that the flying wing is the theoretically optimal layout in aerodynamic terms [1]. However, valuable results can be obtained by considering the design from an aeroelastic point of view.

When aiming to increase efficiency, a typical measure is to increase the aspect ratio. Yet, a long, thin wing will result in larger bending and twisting due to loading, and this will (in common cases) reduce the lift. Other harmful effects of the loading include fatigue and possible fracture due to overloading [2] and fluttering [3]. There are current structural efforts, such as increasing stiffness or topological optimizations [4], made to relieve this effect. But these are costly and difficult to manufacture.

Combining existing demands, developing a wing configuration that maintains both aerodynamic efficiency and improved loading response is necessary. With this initiative, the Peregrine Falcon becomes a source of inspiration and reference. These hunters can reach a maximum speed of 108.2 m/s [5], making them the fastest bird on Earth.

At descent, the Falcon's wings are brought closer to the body [6]. Its minimal wing loading is close to that of solar

drones. But in comparison, while the carbon fiber material used on artificial UAVs is stiffer than bird bones [7][8], the falcons are still capable of higher velocities with similar wing loading [9][10]. From this comparison, it is logical to hypothesize that the unique M-shaped geometry of the Peregrine Falcon's wing might well contribute to its ability to cruise at high speeds. Hence, this research is dedicated to integrating its relevant features into fixed-winged UAV design.

2. Current Research

When differentiating by their flying principles and biological structure, bird wings are classified into four categories: high-speed wing (the pointed wing mostly), active and passive soaring wing, and elliptical wing [11], with the high-speed wing dedicated to taking large aerodynamic loads.

The efficiency of bird wings in their natural configurations is proven. The slotted passive soaring wing can reduce drag and increase lift by over 30% [12]. The gull wings have pressure distribution and efficiency compared to aircraft wings [13]. However, scarcely any study discusses fixed-wing aircraft utilizing bird wing forms and their configurations [14].

Most bird-mimicry drones are flapping ones that adopt both the lift-generating method and the geometry of the bird. The flapping wing can be 27% more efficient on small scales than fixed wings [15]. Notably, the applications of these structures are on small drones, as the lift-drag ratio of fixed-wing drones deteriorates as the scale reduces, making flapping drones an alternate [16][17]. Meanwhile, research also acknowledges that flapping is still an immature technology, with sensor and computation power limitations, power supply and flight duration limitations, inherent instability, and control difficulties that are pending to be solved [16][18].

Since fixed-wing rotor-powered drones are more stable and developed technology, using bio-inspiration to optimize fixed wings remains valuable.

A fixed-winged drone company named *The Drone Bird* [19] provides rotor-powered products for non-intrusive surveillance and bird control. However, designs produced by the company are far from aerodynamically optimized (e.g., a wavy trailing edge without feathers increases drag [20]). Such direct imitation of birds is justifiable for likeness considerations but not performance-optimized.

Summing existing research, static bird wing aerodynamic properties have been experimented on but not widely applied to rotor-powered drones except for more conventional traits. There is also a lack of discussion on the structural effects of those wings with parametric methods. This research proposes a method to integrate bio-inspiration on conventional fixed wings. The properties of this biomimicry design are analyzed and optimized with a parametrized high-speed wing model. It can provide a new way of incorporating biological features into conventional systems.

3. Design and Optimization Process

The section provides an overview of the parametric design process, optimizing the high-speed wing with a set of requirements.

3.1 Parametric Modeling

The high-speed wing configuration of the falcon, as shown in *Figure 1* in its natural state, is parameterized, as shown in *Figure 2*.

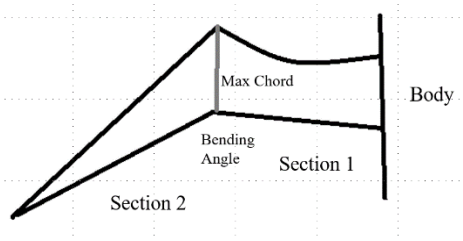

Figure 1. A generic high-speed wing on birds is given in this geometry.

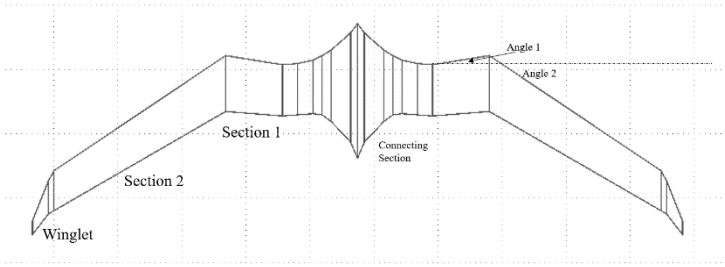

Figure 2. Parametrization of the falcon wing. This geometry is one after optimization.

The transition between sections 1 and 2 occurs at **40.9%** of the wing (closer to the root) - a conclusion based on observing real falcon wings and justifiable with **VLM results**.

3.2 Setting Design Parameters

With the given (averaged) data on peregrine falcons, at a wingspan of 2000 mm, the equivalent takeoff weight should be 3060 grams. Hence, the model is considered with a weight of **3000 grams**.

While there is no available data for the wing area of the falcon, it is known that the peregrine falcon has long, high aspect ratio wings; hence, in analysis, an aspect ratio of approximately 13 is used. *(Later changes are made with systemic considerations on the actual product, but the scaling of chord does not affect aerodynamic properties.*)

3.3 Design Layout

Profili 2 and *XFLR5/Flow5* are the preliminary analytical tools for optimization and adjustment. There are four main steps in the design of the wing (and the planning for the drone as a whole):

- Stabilize;
- Reduce structural shear stress: implementing bird-like distribution of aerodynamic chord distribution;
- Resolve for fluid shear stress: Implement a pointed wing;
- Compensate for lift and further reduce structural bending.

3.4 Parametric Optimization Process

The stabilization process involves the choice of the airfoil and the twisting angles.

HS-510 low-moment airfoil is chosen since it has the highest aerodynamic efficiency amongst airfoils of the HS family. The maximum **thickness is increased to 12.3%** of the chord.

The **MOPSO** module of Flow 5 handles the twisting process. The algorithm runs by designating particles that move on the error landscape. The optimization is carried out in **two rounds**, separately optimizing for cruise drag and lift coefficients.

For the structural effects, let the spanwise position be indicated by y, the wingspan be b, and the local chord length by $c(y)$. Then, the shear force acting on a given point of the wing can be given by

$$S(y) = \int_{y}^{\frac{b}{2}} \int_{0}^{c(y)} (Lift - Gravitation) \qquad (1)$$

The shear force sums up to give the bending moment. The direct effect of shear stress on the wing structure is strain, which is proportional to the tangent of the bending angle.

The chord length of a given point proportionally determines the structural strength. Decreasing the aerodynamic chord will reduce the bending moment, but the actual bending might still increase due to the weakness of the chord and vice versa. When the rearward sweeping angle increases, part of the bending moment is transformed into the torsion moment, twisting the tip forward. In this case, the torsional strength must be compensated for; on a forward-swept wing, this force pitches the airfoil to a higher-loaded state by giving the opposite effect, causing a divergent response.

While human aviation tools conventionally have non-increasing chord lengths moving outward from the root to the tip, this is often not the case on bird wings.

To study the effect of this feature, a force corresponding to CL=0.432 is applied to the optimized wing and compared sets.

Table 1. Responses when force is applied to the wing.

TAPER RATIO	AVE VM (MPA)	MAX VM (MPA)	URES (MM)
0.87	1.158	4.464	18.80
1.09	0.890	3.917	13.03
1.42	0.658	3.899	9.359

Assume that the same amount of lift force is gained, the CoP (center of pressure) and the CoG (center of Gravity) move inward, reducing the lever of equivalent vertical forces, so the bending moment and the torsion moment are reduced.

Studying the distribution of stress demonstrates that while the average stress is reduced, the concentration of stress increases locally, increasing maximum stress. With a smaller mid-wing chord, stress is concentrated along the mid-wing section, so large forces will act on the outer segments as well as the inward ones despite the maximum value being smaller. In terms of eventual bending, the increased chord shows a better result.

Numerically, the TR=0.87 case has a maximum URES value of 18.8 mm, while for TR=1.09, the value is 13.03 mm. For a larger taper ratio, the value continues to decrease. This validates the theoretical statement made above.

Although increasing the mid-wing chord length will improve loading response, it will also decrease the wing's aerodynamic efficiency when exceeding a threshold. As the taper ratio increases from approximately **0.9 to 1.1**, the spanwise pressure distribution becomes more even, indicating an increase in efficiency (consistent with numerical results). Excessively increasing the taper ratio will hinder this improvement and disrupt the distribution as the low AR causes increase in vortex. An optimized position at **1.09** is hence chosen, improving the bending and maintaining efficiency.

The second segment features a less-than-one taper ratio. It is a systemic decision based on efficiency and bending considerations and will not be extendedly discussed here.

Including a **forward sweeping inner segment** is an essential structural trait of the high-speed bird wing layout. When implementing a bent wing feature, the CoG and CoP will be moved inwards to decrease the overall torsion moment, while transforming much of the bending to torsion and increasing the bending. This will reduce the total strain and increase the strain at the specific peak position. Moving the pointed tip excessively forward, however, will deteriorate response since the increased torsion moment will exceed the control limit.

The comparison for displacement 0 mm, 30 mm (chosen case), and 60 mm are analyzed.

Table 2. Response comparison for different displacements

MID-WING DISP (MM)	AVE VM (MPA)	MAX VM (MPA)	MAX URES (MM)
0	1.184	4.728	16.36
30	0.890	3.917	13.03
60	1.264	4.686	17.55

It can be concluded from the data that a structurally optimal solution should be a **slightly forward-swept one**.

While using the forward sweeping feature as a method of further structural optimization, it also provides aerodynamic improvements. In fluid dynamics, the flow shear stress is given by the equation

$$\tau = \mu \frac{\delta u}{\delta h} \qquad (2)$$

Where u is the flow velocity, and h is the height above the boundary. It is proportional to the chord length.

Consider the left wing of the drone. Trailing vortices following the wing spin in a clockwise orientation when viewed from the forward of the drone.

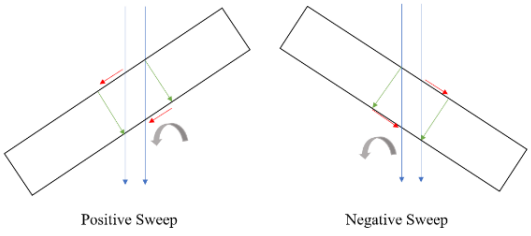

Figure 3. Vortex and spanwise flow on the left wing

The spanwise flow moves from the root towards the tip on a backward-swept wing. This orientation increases the vorticity while pushing the vortex outwards. Vice versa on a forward-swept wing (see *Figure 3*).

Assuming a close-to-elliptical lift distribution, a forward swept wing can be unfavorable as it moves the vortex to the main lift-providing region even though the vorticity is reduced. But on the high-speed wing, implementing the appropriate forward sweeping will reduce the induced drag caused by the long mid-wing chord by canceling vorticity with opposite spin. Through analysis shown in *Figure 4*, CL and CD follow a power relation with the bending angle. This places the favored bending angle threshold at approximately **155 degrees**, and any further bending will not reduce CD effectively.

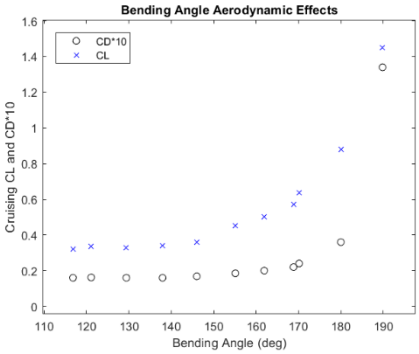

Figure 4. Plot of CL and CD (with VLM method) variation with bending angle, CoG unadjusted, number taken at 3 degrees a.o.a.

Given the purpose of reduction of drag, it is unpreferable to adopt a bending angle of less than 155 degrees (a value near this threshold is eventually taken). Under this constraint, as the first section displacement increases, while the efficiency increases parabolically (sharply before 30 mm, and slows down after that), the bending angle decreases and decreases the CL.

Combining the bending angle and second section fixture (*assuring efficiency, reducing drag as much as possible, and ensuring lift is sufficient*), the full configuration can be obtained by solving for the first segment displacement.

The optimized solution (**30mm**) is more efficient than the straight situation in aerodynamic terms as well as structural terms.

The Pulaski wing configuration, or more generically, the gull-wing configuration, describes a wing with anhedral root chords and dihedral or flat outer section. It can either increase the lift or reduce the drag.

Due to the sideslip effect, the longer dihedral section will increase its lift. The lift-drag ratio and CL and CD curves are parabolic, with the former reaching a maximum value at -2 degrees outward dihedral and the latter reaching a minimum approximately at the same angle. It is logical to obtain the closest dihedral angle to the maximum L/D that satisfies lift requirements, minimizing the drag as much as possible. Meanwhile, the bending moment increases as the wing becomes straight. As to the anhedral, the larger the anhedral angle the first segment adopts, the higher the efficiency. The data from angles of – 5 to 30 degrees on the inner section and -10 to10 degrees for the outer section with 5 degrees variance are compared. Weighing the factors obtain a **first-segment anhedral of 15 degrees and a second-segment dihedral of -6.9 degrees**. This finalizes the configuration of the main wing and its aerodynamic parameters.

The determination of these parameters allows a full determination of the geometry of the bioinspiration high-speed wing.

4. Simulations and Experiments

The evaluation compares the optimized high-speed wing with a straight delta wing under controlled parameters (wing length, lift coefficient and environment data). The procedures are finite element analysis, wind tunnel data validation, and wind tunnel direct comparison.

The finite element analysis uses a force distribution simplification, applying force scaled to the area, which is justified by CWT experiments later. To better compare the wing's status during flight, the result comparison includes attack angles 0 and 3 degrees; the latter is slightly larger than the designated cruising attack angle. The important numerical results are given in the *Table 4.*

Table 3. Elastic comparison

MODEL	AVE VM (MPA)	MAX VM (MPA)	MAX URES (MM)
OPTIMIZED 0 DEG	0.890	3.917	13.03
COMPARED 0 DEG	0.976	3.076	13.70
OPTIMIZED 3 DEG	0.933	4.120	13.07
COMPARED 3 DEG	1.042	3.085	13.73

While the maximum von Mises stress is increased by 27.34% and 33.55% as a result of the stress concentration, the **average and hence total stress are respectively decreased by 8.81% and 10.46%**. As a result of the decreased average von Mises stress, the **tip bending in the two cases is decreased by 5.14% and 5.05%**.

The results of the 0-degree case are plotted to show and compare the spanwise distribution of stress (*Figure 5*) and displacement (*Figure 6*) more closely.

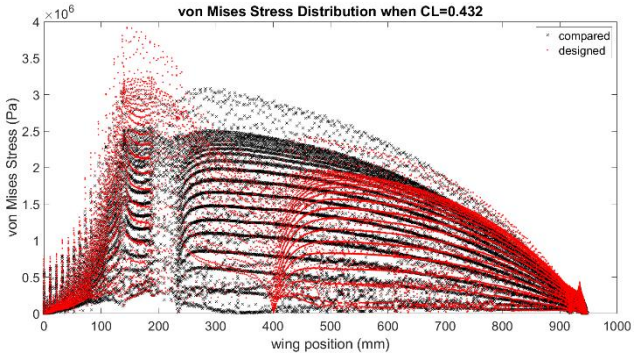

Figure 5. Von Mises stress spanwise distribution indicates that the red points (optimized)experience significant stress reduction from 240 mm to around 700 mm.

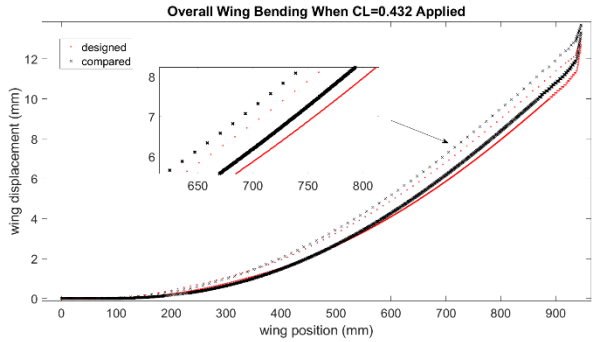

Figure 6. Spanwise distribution of displacement, L.E. and T.E. are plotted; While the red wing (optimized) bends less, it also pitches less than the black wing (compared).

The stress distribution implements a tradeoff between the mid-wing and root chord local stress. This property also indicates that the layout is unsuitable for larger, heavier UAVs. But this is a **desirable exchange for the total decrease on smaller systems**. The bending plot displays a decreased aerodynamic response due to bending and pitching.

Design insight plots are generated to further compare the distribution, An example of the plot is shown in *Figure 7.*

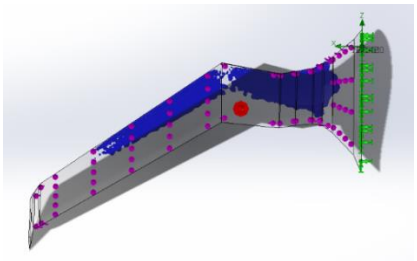

Figure 7. The loading distribution on the wing, 50% high loading area occupies 37.80% of the entire volume.

The result shows a **20.10%** decrease in volume satisfying the constraint. This indicates that the high-speed wing, although causing concentrated stress at the root, decreases the area of the highly loaded region on the wing and improves the overall bending conditions.

The resonance (natural) frequencies of the optimized and delta wing tested at 0 degrees attack angle are respectively 9.4245 Hz and 8.8479 Hz, and 9.4225 Hz and 8,8454 Hz for 3 degrees a.o.a, showing an approximately **6.5% increase in the resonance frequency**. It can be concluded that the optimized wing can cruise at a higher velocity given the same rigidness in material, as its resonance frequency is higher.

The Conditions wind Tunnel experiment act as the validation for the simulation. The wing's aerodynamic properties are tested at the CWT at Shanghai Automobile Wind Testing Centre. In the experiment, half of the wing (chord length doubled, the aerodynamic property remains the same) is constructed and fixed on a steel structure. No direct lift and drag forces are measured since the CWT is not an aeronautic wind tunnel and does not possess the related equipment; instead, pressure and displacements are measured for analysis.

.

Figure 8. A full view of the entire structure in the CWT; the two legs of the frame are stabilized with two sandbags, each weighing 40 kg, and two fixing weights are placed at the back to prevent sliding. The tubes for the pressure measurement are led down on the frame (fixed to the frame by the tapes) to the ground.

The pressure sensors let in airflow and measure the pressure. It is connected to the computation and transmission module by soft tubes led down to the ground from the sensors on the wings. A pair of laser sensors are installed at the tip section of the wing. They are approximately on the same aerodynamic chord, so the displacement they demonstrate will help indicate the aerodynamic twisting effect and oscillations on the wing.

Wind speeds of 40 km/h, 60 km/h, 70 km/h, 75 km/h, 80 km/h, 85 km/h, and 90 km/h are tested under 26 degrees Celsius in the wind tunnel two times, each time collecting 60 seconds of analyzed data.

An example of the raw data obtained is shown in *Figure 9*. The sample rate is 100 Hz, and the data is taken over one minute, summing up to 6000 data sets.

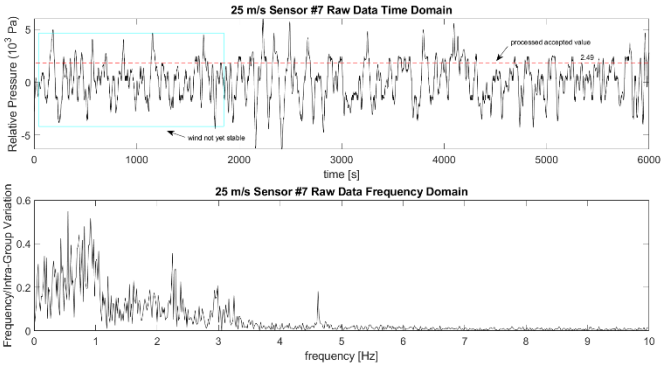

Figure 9. Raw data and frequency domain for 25 m/s sensor number 7 at 100 Hz sample rate.

As indicated in the time plot, the data obtained oscillates instead of a constant value. This is a result of numerous factors, including environmental noise, sensor installation methods, and sensor systematic error. To find the actual pressure measurement, knowing that the relative pressure must be positive, only the local maxima within the selected

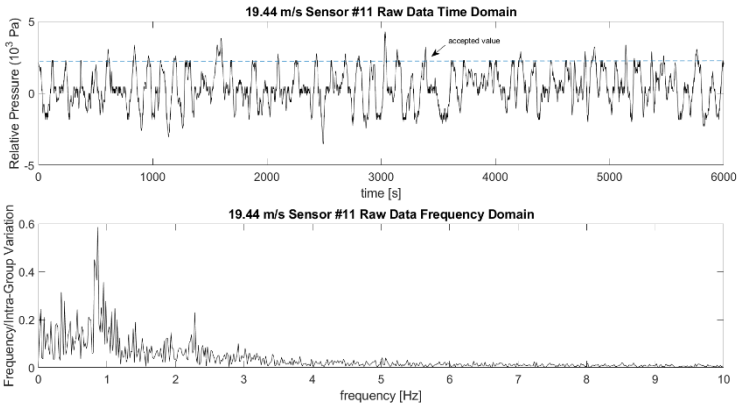

calculation range are taken as considered data and averaging over these maxima gives an estimation of the accepted measurement value shown in the demonstration by the dashed line.

Figure 10. Raw data for 70 km/h. It can be shown that under a lower velocity, the variation of pressure due to fluttering is reduced largely.

For comparison, another set of raw data is plotted in *Figure 10*. At the lower velocity, the data is significantly smoother (less variation in the local maxima points, which indicate useful values.

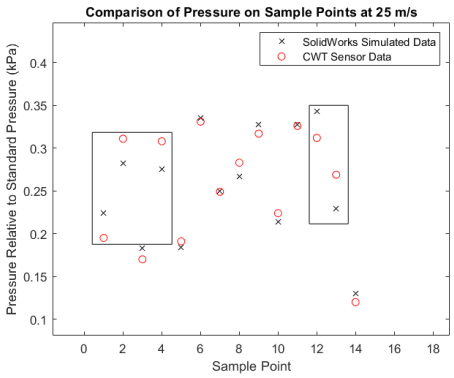

Figure 11. Pressure sample point comparison at 25 m/s, the experimental and theoretical data differ by 6.89%, and points where significant differences are observed (over 10%) are boxed.

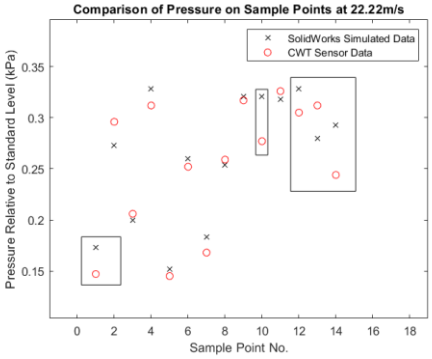

Figure 12. Pressure sample point comparison at 22.22 m/s, the experimental and theoretical data differ by 7.27%.

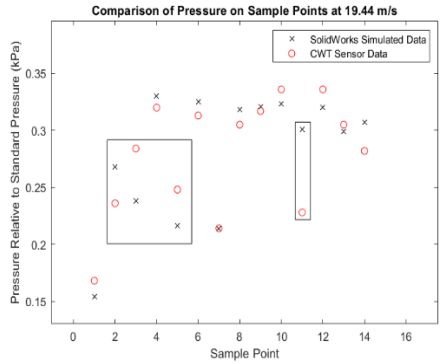

Figure 13. Pressure sample point comparison at 19.44 m/s, the experimental and theoretical data differ by 7.90%.

Comparing the data for 25 m/s, 22.22 m/s, and 19.44 m/s with the results obtained from probes in SolidWorks flow simulation in *Figures 11*, *12*, and *13* shows that the data fit relatively well, featuring deviations majorly at the tip and root sensors. Installation factors can justify this. The average absolute value of the error for these **three sets of data is 6.89%, 7.27%, and 7.90%, respectively**. *This is an acceptable value* up to industry standard [21] and demonstrates that the simulation is effective.

It is also observed that as the velocity increases, the accuracy of the data increases. *The maximum projected error is 8.57% at 12.39 m/s*.

For the displacement data from the laser sensors, the raw data is processed into relative data to study the amplitude and frequency of the fluttering. Results fit well with theoretical curve types.

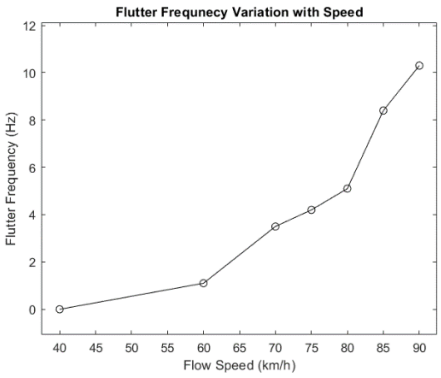

Figure 14. Flutter frequency variation with speed, MATLAB gives R-square = 0.9854 fit curve with power function.

According to the processed data on flutter frequency in *Figure 14*, the resonance frequency is estimated to be **18.4 Hz**. Inputting the data for foam material, the frequency analysis of the SolidWorks Simulation module puts the frequency at 15.32 Hz. Since thin carbon tubes (5 mm diameter) are added for structural support and wire organization, it is justifiable that the expected resonance frequency in the experiment is slightly higher.

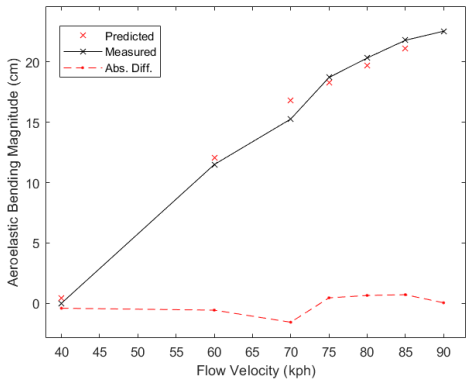

Figure 15. Aeroelastic bending comparison, the maximum difference is 9.4%, the average value is 3.7%,

The aeroelastic bending can also be compared as in *Figure 15*. The experimented data only shows a **3.7%** variance on average with the simulation data.

CWT experiment indicates that the fluid calculation and

static force approximations and assertions made for calculation are valid and **can fit with empirical data** to produce meaningful results.

While the data validation is complete, a direct experimental comparison of the optimized wing and the conventional one is made. Using 1:53 SLA high accuracy 3D printed models for testing, a micro-scale desktop wind tunnel (abbrev. DWT, *shown in Figure 16*) capable of voltage speed control and a maximum windspeed of 6 m/s is constructed.

Figure 16. Testing condition of the desktop wind tunnel.

The raw data are presented in the form of images - frames drawn from the recorded 60-second video from the camera. The 120fps frame rate allows the calculation of any frequencies below 120 Hz. The oscillation is measured graphically with digital software (hence, it is in 'units' only). The voltage is set as the independent variable as it varies linearly with the wind speed. The experiment repeats a four-group set three times, each consisting of a 0-degree and 5-degree situation for both models.

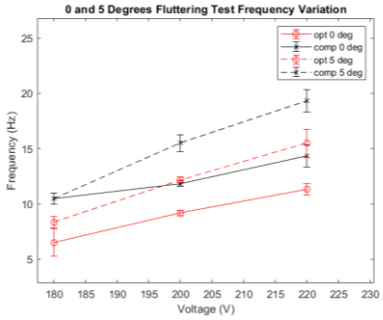

Figure 17. Flutter frequency variation with voltage.

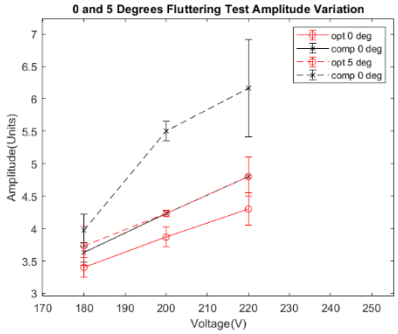

Figure 18. Flutter amplitude (units derived from image analysis) variation with voltage.

Experimental data indicates that under the same flow velocity, the *fluttering amplitude* of the designed model can be reduced by as much as **more than 20%** and the *fluttering frequency* by as much as **more than 17%**. It can be shown that for below 200 V, there is a sharp decrease in frequency and amplitude. In contrast, the decrease rate reduces after surpassing 200 V. This implies that the straight wing enters flutter first.

The DWT experiment proves the validity of the aeroelastic improvement of the high-speed wing while maintaining aerodynamic efficiency. Despite its inaccuracy due to structural deviations, singular flow regulation device, and filming conditions, it can produce a meaningful comparison with data within reasonable ranges.

The three experiments combine to prove that the high-speed wing improves loading responses without any efficiency costs.

5. System Engineering

The data and images below demonstrate a UAV system developed with the result of this research. It is constructed with foam, carbon fiber, and engineering plastic materials.

Table 4. System specifications

TERM	DATA	UNIT
A.R.	7.8	/
WINGSPAN	1890	mm
LENGTH	840	mm
L/D RATIO	19.8	@19m/s
MTOW	5200	g
PLD MAX	2845	g (@1.22hrs 83 km)
VC MIN	19	m/s (@MTOW)
VS	14	m/s
V MAX	35	m/s
VNE	46	m/s
DUR MAX	5.6	hrs (MTOW, 1220g pld)
RANGE MAX	383	km (MTOW, 1220g pld)
SYSTEM COST EST.	2950	$

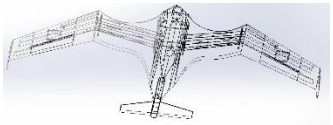

Figure 19. SW model

Figure 20. Actual model

Comparatively, a Boeing 737 airliner has an aspect ratio of 8.8 [22] and a lift-drag ratio of 18.2 [23]. This indicates that the wing designed has high aerodynamic efficiency compared to commercialized counterparts aside from its aeroelastic benefits.

6. Conclusion

6.1 Results

Through the bioinspiration from peregrine falcon wings, the process for developing a pointed wing configuration for fixed-winged drones is established, and approximation-based analyses show an **8.8% to 10.5% decrease in bending moment, 5% decrease in displacement, and 20.10% decrease in high loading area** on the wing compared to the aerodynamically most efficient flying wing. The CWT and micro DWT experiments have proved that the calculations with approximations are consistent with realistic situations, and the conclusions developed accordingly are valid.

It is believed that this design when utilized on small drones, provides a **novel, cost-effective method** to increase the VNE for drones with related design requirements. Drones adopting this configuration can use lighter support structures and accelerate **to higher maximum speeds**, depending on the preference of the situation.

The decrease in aerodynamic bending is also predicted to **improve the structural endurance** as less fatigue will be experienced.

6.2 Limitations

While obtaining expected improvements, there are some drawbacks to this configuration.

The most important side effect is the **low responsiveness of the lift to control**, hindering (especially) the climbing performance of the aircraft. This issue is innate, as the form of the wing imitates a gliding bird, not a climbing one, and hence is **limited in its biomimicry**. One possible solution is implementing an adjustable structure to configure the bending angle to best fit the desired cruising or climbing situation. The mimicry also develops the need for a **corresponding unique structural solution**, as given briefly in the system design. requiring some changes to the traditional structural designs.

Although these limitations exist, they do not undermine the effective benefits brought by this configuration.

6.3 Implications

A high-speed wing form **improves aeroelastic responses without decreasing aerodynamic efficiency**.

One way to view the improvement is the **decrease in structural weight.** When providing the same lift, the need for structural strengthening is reduced. Moreover, the reduction is taken further with a slight decrease in wingspan.

Another way to interpret the result is that with the same structural strength, the optimized high-speed wing is capable of a higher speed. That is, it **improves maneuverability**.

The configuration allows small UAVs of such design to gain better performance in tasks including survey, rescues, and communications.

7. Acknowledgements

This research was initiated on April 4th, 2023, and is completed on September 14th, 2023. Initially oriented as a design project, it has gone through major transformations in the process.

Professor Huang, joined the guidance of my project in mid-July. He brings me valuable theoretical, and systemic suggestions that kept my work valid and on track.

I have also received assistance from several aeronautics and control professional: Prof. Li Guangxia of NUAA, Prof. Kong Xingwei of AFEU, Dr. Liang Qiang of SAST, Dr. Jonathan Jiang of NASA JPL, PMTS Xiao Lianghe of AVIC (Chengdu), Mr. David S. Jeon of Caltech, and Mr. Yang Yu of TUTE, as well as a few whose name are not written here. The experiment in SAWTC was made possible by Dr. Wu Duan and Dr. Fang Liang, as well as the entire CWT engineering crew.

Lastly, I wish to thank my family for their utmost support and understanding for my work. It would not be possible to complete this project without their devotion.

References

[1] Hamada, A. Sultan, and M. M. Abdelrahman, “Design, build and fly a flying wing,” *Athens Journal of Technology & Engineering*, vol. 5, no. 3, pp. 223–250, Aug. 2018, doi: 10.30958/ajte.5-3-2.

[2] X. Katifes, “Structural analysis, fatigue analysis and optimization of aircraft wings,” *ResearchGate*, Mar. 2016, doi: 10.13140/RG.2.1.1256.6647.

[3] Wang Libo, Tang Chu, Yang Chao. Dynamic Stability Analysis of a Flying Wing Considering the Rigid-Elastic Coupling Effects. *Journal of Northwestern Polytechnical University*, 2017, 35(6): 1096-1104.

[4] LYU Ji'nan, GUO Li, FAN Xueling, CHEN Gang, LIU Ziqiang. Topology optimization of high-aspect-ratio wing section considering aeroelastic effect[J]. *Acta Aerodynamica Sinica*, 2018, 36(6): 1047-1051. doi: 10.7638/kqdlxxb-2018.0024

[5] Ponitz, A. Schmitz, D. Fischer, H. Bleckmann, and C. Brücker, “Diving-Flight Aerodynamics of a Peregrine Falcon (Falco peregrinus),” *PLOS ONE*, vol. 9, no. 2, p. e86506, Feb. 2014, doi: 10.1371/journal.pone.0086506.
[6] J.-M. Tsang, “The fastest animal on Earth ‘The Peregrine Falcon’ | *Bio-aerial Locomotion* 2011,” Oct. 07, 2011.
[7] Themes U. Mechanical properties of bone. *Musculoskeletal Key*. Published May 22, 2017.
[8] Collins MN, Culebras M, Ren GK. The use of lignin as a precursor for carbon fiber–reinforced composites. In: *Elsevier eBooks*.; 2022:237-250. doi:10.1016/b978-0-12-823702-1.00011-6
[9] K. Mullins, “Peregrine Falcon Speed: How Fast Is a Peregrine Falcon?”, *Misfit Animals*, Jun. 09, 2022.
[10] “SUNBIRDS SB4 PHOENIX USER MANUAL PDF download,” *ManualsLib*, Feb. 2020, [Online].
[11] S A. Volant adaptation in animals. *Zoology Notes*. Published July 25, 2016.
[12] P. B. Salunkhe, Y. Wu, and H. Tang, “Aerodynamic performance improvement of a wing model using an array of slotted synthetic jets,” *Journal of Fluids Engineering-transactions of the Asme*, vol. 142, no. 10, Jun. 2020, doi: 10.1115/1.4047397.
[13] Jia, W., Hua, X., Shi, J., & Zuo, C. (2020). Aeroelastic Analysis on Bionic Gull Wing Based on Fluid-Solid Coupling Methods. *Journal of Ordnance Equipment Engineering*.
[14] S. V. Sandapeta and S. K. Parre, “Conceptual Design and analysis of Flying Wing Drone,” *ResearchGate*, Aug. 2018, [Online].
[15] “To flap, or not to flap? Flapping wings can be more efficient than fixed wings, study shows | Cornell Chronicle,” *Cornell Chronicle*, Sep. 29, 2009.
[16] G. De Croon, “Flapping wing drones show off their skills,” *Science Robotics*, vol. 5, no. 44, Jul. 2020, doi: 10.1126/scirobotics.abd0233.
[17] M. F. Abas, A. S. B. M. Rafie, H. Yusoff, and K. A. Ahmad, “Flapping wing micro-aerial-vehicle: Kinematics, membranes, and flapping mechanisms of ornithopter and insect flight,” *Chinese Journal of Aeronautics*, vol. 29, no. 5, pp. 1159–1177, Oct. 2016, doi: 10.1016/j.cja.2016.08.003.
[18] D. Lentink, et al., "Bioinspired aerial robotics: Optimal morphing wings and flight control," *Bioinspiration & Biomimetics*, vol. 11, no. 2, 2016, pp. 025002-025002.
[19] “The Drone Bird Company | Unmanned aircraft systems and wildlife management.” https://www.thedronebird.com/
[20] S. J. Yang and J. D. Baeder, “Aerodynamic Drag and Aeroacoustic Noise Mitigation of Flatback Airfoil with Spanwise Wavy Trailing Edge,” *American Institute of Aeronautics and Astronautics*, Jan. 2015, doi: 10.2514/6.2015-0993.
[21] What is the suitable and acceptable error variations between the CFD results and experimental data? - FAQS.TIPS.
[22] Aerodynamic Data Base, Wings Aspect-Ratios. *Aerodyn*. Published September 3, 2020.
[23] Memon O. What Factors Determine The Performance Of A Boeing 737 MAX When Cruising? *Simple Flying*. Published December 25, 2022.

Hanyue Shen
High school IBDP student at Shanghai Pinghe School.